Supporting Information

Polydopamine coated bimetallic ZIFs Derivatives as air cathode for acidic Zn–air batteries with the super-high potential

Zhenzhen Chi ,[‡a] Yingying Feng ,[‡a] Yiru Ma ,[a] Dezhi Kong ,[a] Huixiang Yin ,[a] Shaoxiang Li ,[b] Lin Li ,[c] Ziyang Guo [*a] and Lei Wang [*a, b]

a Key Laboratory of Eco-chemical Engineering, Taishan Scholar Advantage and Characteristic Discipline Team of Eco-Chemical Process and Technology, College of Chemistry and Molecular Engineering, Qingdao University of Science and Technology, Qingdao 266042, China.

b College of Environment and Safety Engineering, Qingdao University of Science and Technology, Qingdao 266042, China.

c Research Center for Green Printing Nanophotonic Materials School of Materials Science and Engineering Suzhou University of Science and Technology, Suzhou, 215009, China.

** Corresponding author. Tel & Fax: 0086-0532-84023409*

E-mail address: inorchemwl@126.com (Wang L); zyguo@qust.edu.cn (Guo Z)

‡ Zhenzhen Chi and Yingying Feng contributed equally to this work.

Material Preparation

Materials

Cobalt nitrate hexahydrate (Co $(NO_3)_2 \cdot 6H_2O$, 99 %), 2-Methylimidazole was purchased from MACKLIN Reagent. 2-methylimidazole (99 %) was purchased from J&K Scientific Reagent. Cetyltrimethylammonium Bromide (CTAB) was purchased from Tianjin BODI Reagent. Potassium hydroxide (KOH, 90 %), Dopamine hydrochloride and Tris-Hydrochloride Buffer were purchased from Aladdin Reagent. Sulfuric acid (H_2SO_4, 98 %) was purchased from Yantai Far Eastern Fine Chemical Co., Ltd. Bipolar membrane was brought from Huamo Tech. Co., Ltd. Pt/C and Ruthenium dioxide (RuO_2) were purchased from Alfa Aesar (China) Chemical Co., Ltd. Other chemicals were from Sinopharm Chemical Reagent Corp. All chemicals were used as received without further purification.

Preparation of Co/Zn-ZIFs

Co/Zn-ZIFs nanocrystals were synthesized by co-precipitation method. Typically, 4546 mg 2-methylimidazole was dissolved in 70 mL deionized water to form a clear solution. Additionally, $Zn(NO_3)_2 \cdot 6H_2O$ (223.12 mg), $Co(NO_3)_2 \cdot 6H_2O$ (72.76 mg) and CTAB (5 mg) were firstly dissolved in 10 mL deionized water and then were quickly transferred into the 2-methylimidazole containing solution. Subsequently, the above mixed solution was further stirred vigorously for 20 min and then was allowed to stand use at room temperature for 24 h. After that, the precipitate was obtained through centrifugation and further repeatedly washed with deionized water and ethanol (volume ratio of 1:1) for several times. Finally, the residual sample was dried in a vacuum at

80°C overnight. The resulting powder is named as Co, Zn bi-metallic ZIF-67 (Co/Zn-ZIFs). Moreover, ZIF-67 nanocrystals were prepared trough the same procedure except that only Co $(NO_3)_2 \cdot 6H_2O$ (291.04 mg) was added as the metal source.

Preparation of NC@Co-HPNC

The precursor PDA@Co/Zn-ZIFs is prepared by coating a layer of polydopamine on the surface of Co/Zn-ZIFs by on-site polymerization. In a typical procedure, the commercial Tris-hydrochloride buffer is diluted to 10 mM (pH=8.5). The as-prepared Co/Zn-ZIFs sample (200 mg) was added to 200 mL Tris-hydrochloride diluent and further sonicated to form a uniform suspension. In addition, 20 mg dopamine hydrochloride was dissolved in the mixed solvent of 4 mL ethanol and 6 mL deionized water. Then, the obtained dopamine hydrochloride based solution was subsequently added to the above suspension and further stirred vigorously for 40 min. Afterward, the precipitate was collected through centrifuging and washing with deionized water/ethanol (volume ratio of 1:1) for several times, which was further dried in a vacuum at 80 °C overnight. The resulting product was denoted as PDA coated Co/Zn-ZIFs (PDA@Co/Zn-ZIFs). Finally, the obtained PDA@Co/Zn-ZIFs was calcined in the nitrogen atmosphere at 900°C for 2 hours to form Co nanoparticles encapsulated in highly porous N-doped carbon nanocube (denoted as NC@Co-HPNC). For comparison, Co nanoparticles embedded in N-doped carbon nanocube (Co-NC) and Co nanoparticles encapsulated in highly porous N-doped carbon nanocube (Co-HPNC) were prepared by pyrolyzing ZIF-67 and Co/Zn-ZIFs in the same way, respectively.

Assembly of acid-base dual electrolyte based Zn–air battery

Firstly, 30 wt % Ketjenblack (KB), 60 wt % NC@Co-HPNC powder and 10 wt % poly tetra fluoroethylene (PTFE) binder were was dispersed in the isopropanol solvent to form slurry. Next, the commercialized waterproof membrane with a diameter of 14 mm was slightly pressed on the stainless steel mesh to form waterproof layer under the pressure of 10 MPa. Additionally, the (KB + NC@Co-HPNC + PTFE) slurry was rolled into a membrane with the same diameter of 14 mm, and finally pressed on the surface of the waterproof layer coated stainless steel mesh under a pressure of 40 MPa to form the NC@Co-HPNC based electrode. The NC@Co-HPNC based electrode was dried for 12 h at 80 ℃ under vacuum to remove residual solvent. The assembly of acid-base dual electrolyte based Zn–air battery using NC@Co-HPNC cathode is as follows: firstly, we designed the home-made two-chamber battery that contains the cathode chamber and anode chamber, respectively. The as-prepared NC@Co-HPNC based electrode was used as air cathode in the cathodic chamber filled with 1M H_2SO_4 electrolyte, while the Zn film was applied as the anode in the anodic chamber filled with 6M KOH solution. Moreover, there is a bipolar membrane between the cathodic chamber and anodic chamber, which is aimed to separate the acidic and alkaline solution.

The mechanical recharging processes

The Zn–air battery using NC@Co-HPNC catalyst was discharged at 5 mA cm^{-2} for 24 h. After this process, the battery was disassembled in the air. Then, the NC@Co-HPNC-based cathode was washed with water and ethanol. Next, the battery was reassembled with a new Zn anode and KOH electrolyte for another 24-hour discharge process.

The reaction mechanism of alkaline or acid-base dual electrolyte based Zn–air batteries

In the conventional alkaline Zn–air batteries, the reaction mechanism is based on the following equations:

The oxygen reduction/evolution reaction (ORR/OER) at the air cathode according to equation 1:

$$O_2 + 2H_2O + 4e^- \leftrightarrow 4OH^- \quad 0.40\ V\ vs\ SHE \tag{1}$$

The electrochemical reactions occurring at the Zn electrode is also summarized in equation 2:

$$Zn + 4OH^- \leftrightarrow Zn(OH)_4^{2-} + 2e^- \quad -1.199\ V\ vs\ SHE \tag{2}$$

In the acid-base dual electrolyte based Zn–air cells, the reaction mechanism is based on the following equations:

The oxygen reduction/evolution reaction (ORR/OER) at the air cathode under acidic conditions according to equation 3:

$$O_2 + 4H^+ + 4e^- \leftrightarrow 2H_2O \quad 1.23\ V\ vs\ SHE \tag{3}$$

The electrochemical reactions occurring at the Zn electrode in the alkaline electrolyte is also summarized in equation 4:

$$Zn + 4OH^- \leftrightarrow Zn(OH)_4^{2-} + 2e^- \quad -1.199\ V\ vs\ SHE \tag{4}$$

Therefore, by coupling the Zn anode in alkaline electrolyte with the air cathode in acidic electrolyte, the resulting acid-base dual electrolyte based Zn−air cell can provide a high theoretical voltage of ~2.43 V, which is obviously higher than that of the conventional alkaline Zn–air batteries (~1.60 V).

Measurement of ionic conductivity

It can be detected that the tested electrolyte resistance is obtained from the intercept of the Nyquist plot with the real axis. The conductivity σ of the prepared electrolyte membranes are obtained by using the following equation:

$$\sigma = l/RS$$

Here, R is the measured resistance of the prepared electrolyte membrane, l is the thickness of the

prepared electrolyte membrane between counter SSS electrodes (0.46 mm), and S is the contact area of the prepared electrolyte membrane and the electrodes (2.5434 cm^2).

Physical characterization

The morphology and structure of materials were studied via Scanning electron microscopy (SEM, JSM-6390 JEOL) and Transmission electron microscopy (TEM, JEM-2100F). Specific surface areas were calculated by the Brunaure Emmert Teller method. Pore volumes and sizes were estimated from the pore-size distribution curves from the adsorption isotherms using the Barrett Joyner Halenda method. X-ray diffraction (XRD) was conducted on a Bruker D8 Focus power X-ray diffractometer with Cu-Kα radiation. X-ray photoelectron spectroscopy (XPS, Kratos Analytical Inc) was used to investigate the chemical composition. Electrochemical performance was measured on Gamry RDE710 rotating electrode (Gamry instrument co., LTD, America).

Electrochemical characterization

All electrochemical measurements were measured in a conventional three-electrode system using an electrochemical workstation (CHI 660E). A rotating electrode with an area of 0.196 cm^{-2}, a Hg/HgO (saturated 1.0 M KOH solution, alkaline condition) electrode or saturated calomel (saturated KCl solution, acidic condition) electrode and platinum sheet were applied as working electrode, reference electrode and counter electrode. To prepare working electrodes, 2 mg of the catalyst (NC@Co-HPNC, RuO_2 or Pt/C) was dispersed in ethanol (275 μL) and Nafion (25 μL) by ultrasound for 30 minutes to obtain homogeneous dispersion. 10 μL of the suspension was deposited on the 5 mm diameter rotating disk electrode and allowed to dry

naturally. The payload of all catalysts was ~ 0.34 mg cm^{-2}.

For ORR test, the polarization curves were collected at different rotating electrode speeds (400 ~ 2500 rpm) in 0.1 M KOH at 5 mV s^{-1}. The LSV curve for OER was employed in saturated 1 M KOH at the same sweep rate. For tests requiring oxygen or nitrogen atmosphere, gas should be supplied into the electrolyte for more than half an hour to achieve the N_2/O_2-saturated solution. In addition, gas should be slowly supplied into the testing system.

All testing potential differences between the working electrode and Hg/HgO electrode can be converted to the voltage differences between the working electrode and a reversible hydrogen potential (RHE) based on the following formula: .

The overpotentials were determined by the following formula: $\eta = E\,(vs.\,RHE) - 1.23$. O_2/H_2O equilibrium at 1.23 V *vs.* RHE.

For H_2O_2 yield, the RRDE was carried out at 1.5 V under 1600 rpm. The percentage of H_2O_2 yield and the number of transfer electron (n) can be acquired according to formulas: $H_2O_2(\%) = 200 \times I_r/N(I_d + I_r/N); n = 4 \times I_d/(I_d + I_r/N)$. I_d represents disk current, I_r represents ring current, and N represents ring collection efficiency of RRDE (0.37).

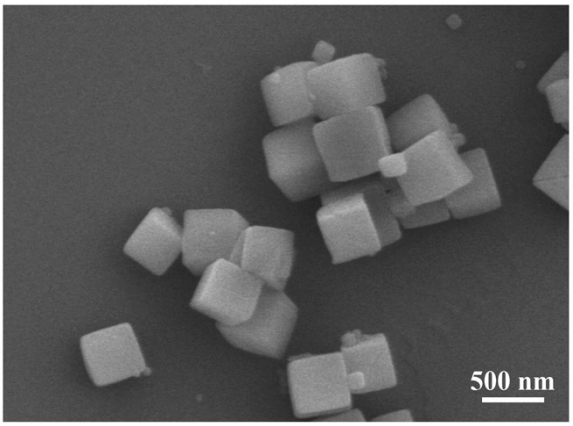

Fig. S1 SEM image of Co-ZIFs.

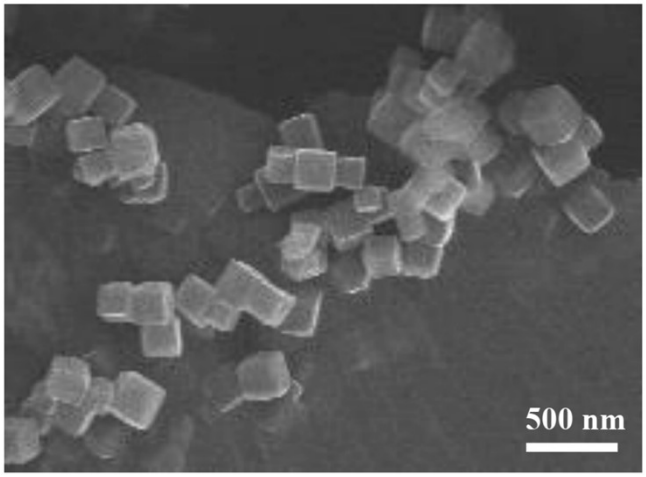

Fig. S2 SEM image of Co/Zn-ZIFs.

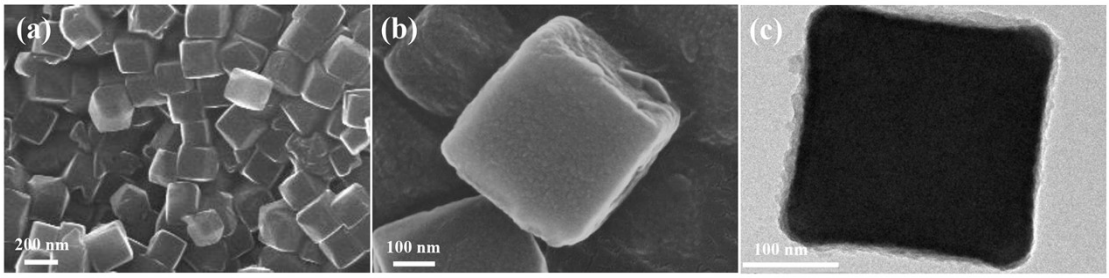

Fig. S3 (a, b) SEM and (c) TEM images of PDA@Co/Zn-ZIFs.

As shown in **Fig. S3**, there is an additional thin coating layer on the surface of PDA@Co/Zn-ZIFs compared with Co-ZIFs and Co/Zn-ZIFs, , which suggests the successful introduction of PDA layer.

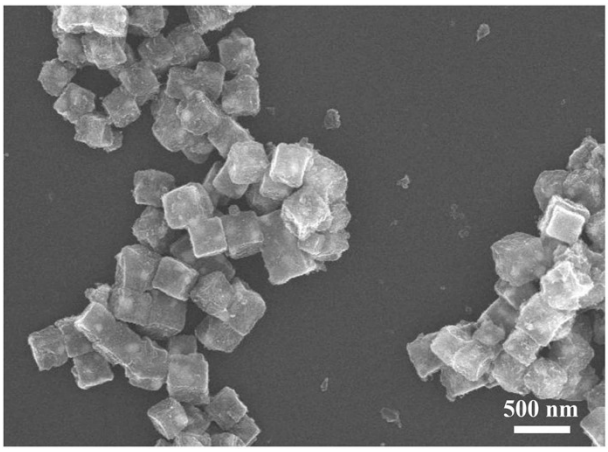

Fig. S4 SEM image of Co-NC.

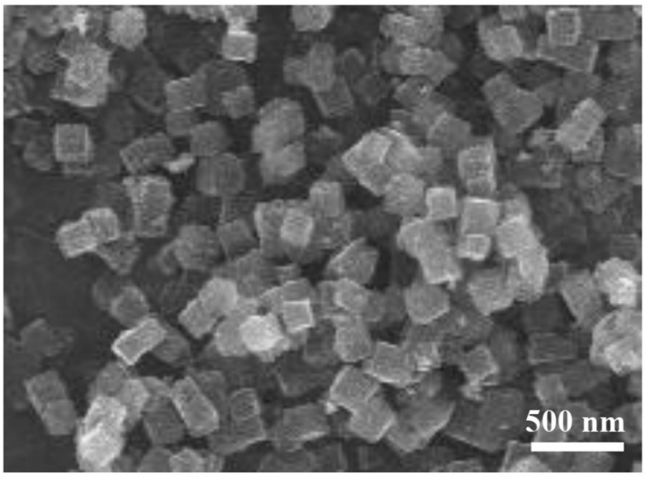

Fig. S5 SEM image of Co-HPNC.

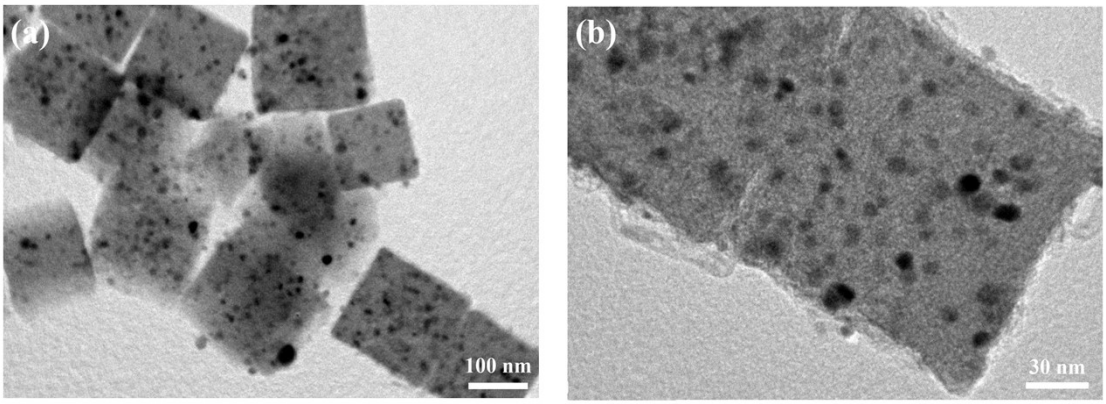

Fig. S6 TEM images of Co-HPNC.

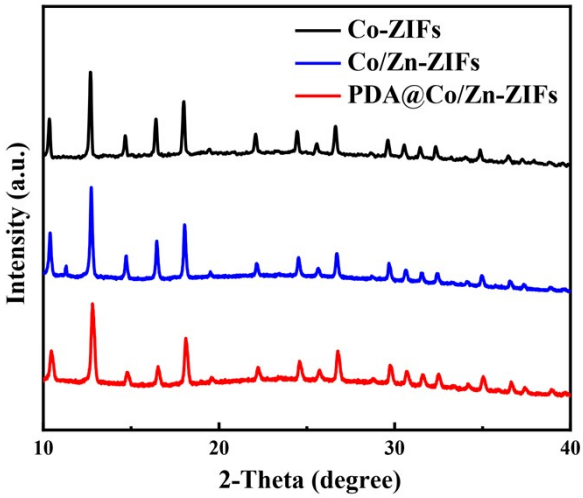

Fig. S7 XRD patterns of Co-ZIFs, Co/Zn-ZIFs and PDA@Co/Zn-ZIFs.

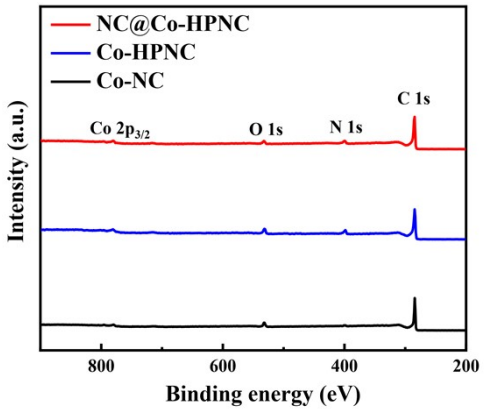

Fig. S8 X-ray photoelectron spectroscopy (XPS) survey spectrum of Co-NC, Co-HPNC and NC@Co-HPNC.

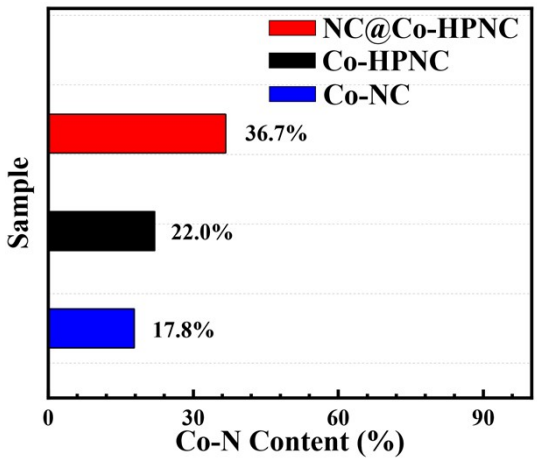

Fig. S9 Percentages of Co-N species calculated from the Co 2 p spectra for Co-NC, Co-HPNC and NC@Co-HPNC.

As shown in **Fig. S9**, the surface Co-N contents which are beneficial to OER performance are 17.8%，22.0% and 36.7% in Co-NC, Co-HPNC and NC@Co-HPNC, respectively.

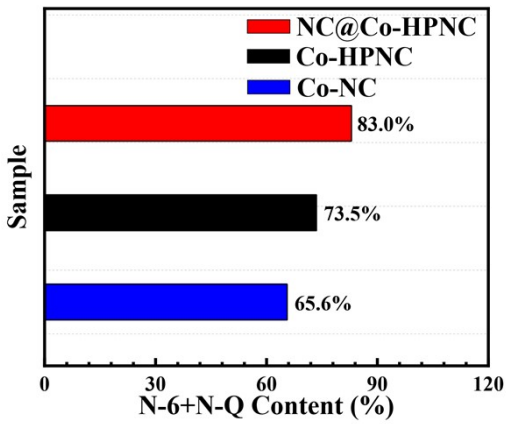

Fig. S10 Percentages of N-6 + N-Q from N 1s spectra for Co-NC, Co-HPNC and NC@Co-HPNC.

It can be shown from **Fig. S10** that the relative composition of N-6 + N-Q that are favorable for ORR performance in NC@Co-HPNC (83.0%) is significantly higher than these of Co-HPNC (73.5%) and Co-NC (65.6%).

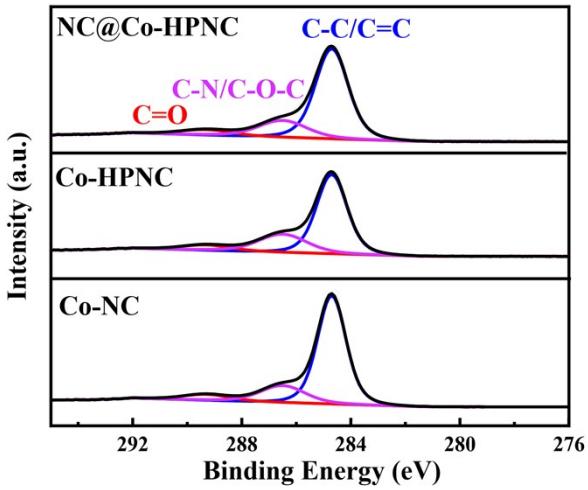

Fig. S11 high-resolution XPS spectra of C 1s of NC@Co-HPNC, Co-HPNC and Co-NC.

Fig. S11 shows that the high-resolution C 1s spectrum can be resolved into three individual peaks, which are corresponding to C-C/C=C (284.7 eV), C-N/C-O-C (286.5 eV) and C=O (289.3 eV), respectively. The existence of the C-N bond further proves the successful doping of N in these carbon matrixes, which can provide more active sites for electrocatalysis.

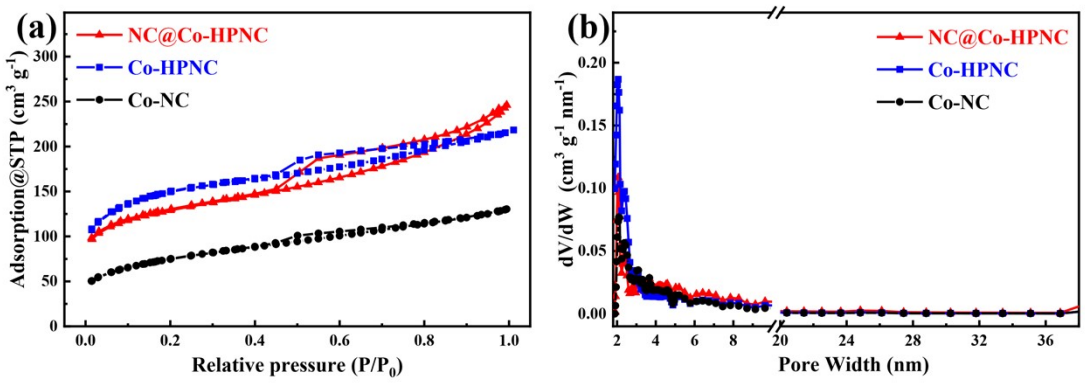

Fig. S12 (a) N_2 adsorption-desorption isotherms and (b) pore-size distribution curves of NC@Co-HPNC, Co-HPNC and Co-NC.

As shown above, **Fig. S12a** shows that the N_2 adsorption-desorption isotherms of all these Co-based derivatives exhibit the obvious hysteresis loops at the medium and high pressure ranges, indicating the co-existence of the mesopores and micropores in all three samples. There are the similar pore sizes centred at around 1.8-2.9 nm in all the Barrett-Joyner-Halenda (BJH) pore size distributions shown in **Fig. S12b**, further confirming considerable microporous and mesoporous structures in three Co-based materials.

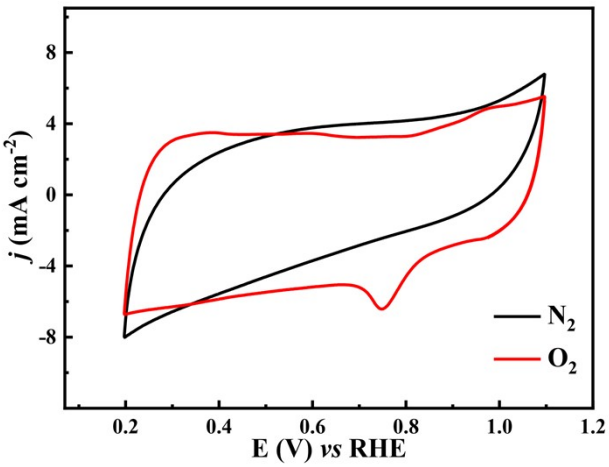

Fig. S13 CV curves of NC@Co-HPNC in N_2 and O_2-saturated 0.1 M KOH solution.

The CV measurement is tested in 0.1 M KOH aqueous solution with saturated O_2 or N_2. As depicted in **Fig. S13**, a well-defined cathodic peak emerged at ~ 0.74 V vs. reversible hydrogen electrode (RHE) in O_2-saturated KOH solution, but no noticeable reduction peak was seen for the electrolyte filled with N_2, indicating a pronounced ORR activity of NC@Co-HPNC.

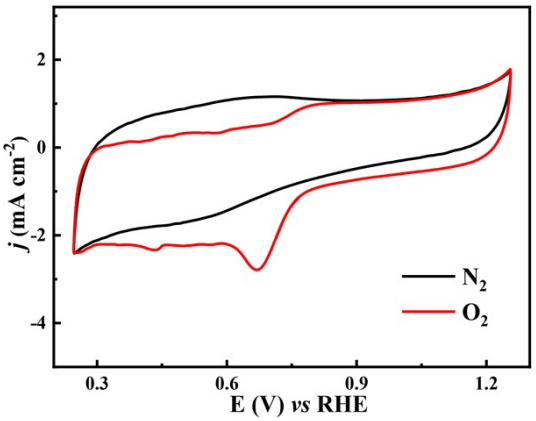

Fig. S14 CV profiles of the NC@Co-HPNC catalyst in the 0.5 M H_2SO_4 electrolyte saturated with pure N_2 or O_2 gas.

As shown in **Fig. S14**, The CV curve of NC@Co-HPNC in 0.5 M H_2SO_4 saturated with O_2 gas presents an obvious cathodic peak at 0.67 V, but no peak emerging in N_2-filled acid solution, preliminarily confirming that NC@Co-HPNC still has ORR activity under acidic condition.

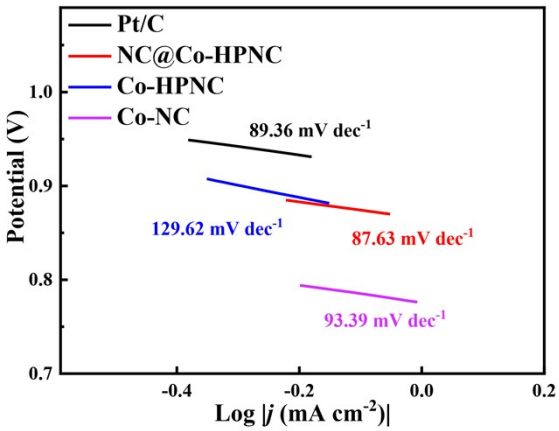

Fig. S15 corresponding Tafel plots of LSV curves for NC@Co-HPNC, Co-HPNC, Co-NC and Pt/C for ORR catalytic activity in O_2-saturated 0.1 M KOH solution with a RDE (1600 rpm).

As shown in **Fig. S15**, the Tafel slope of NC@Co-HPNC, Co-HPNC, Co-NC, and Pt/C catalysts are 87.63, 129.62, 93.39 and 89.36 mV dec^{-1}, respectively, which reveals a high intrinsic activity of NC@Co-HPNC towards ORR.

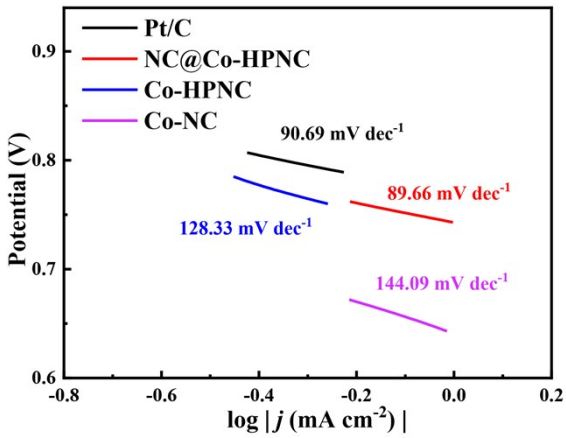

Fig. S16 corresponding Tafel plots for LSV polarization curves of the Pt/C, NC@Co-HPNC, Co-HPNC and Co-NC catalysts for ORR activity in 0.5 M H_2SO_4 solution saturated with pure O_2 under 1600 rpm.

As revealed in **Fig. S16**, the Tafel plot of NC@Co-HPNC is 89.66 mV dec^{-1}, which are much better than these of the Co-HPNC and Co-NC catalysts, and even comparable to those of Pt/C electrocatalyst (90.69 mV dec^{-1}). These results further indicate the high intrinsic ORR activity of NC@Co-HPNC under acidic environment.

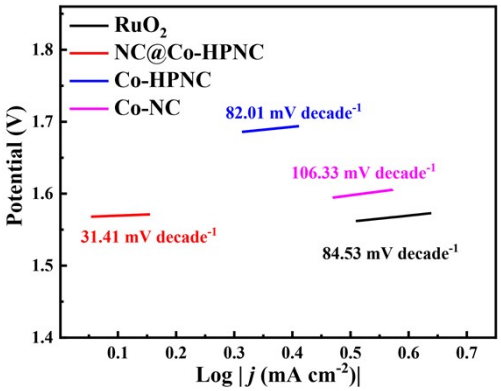

Fig. S17 corresponding Tafel plots for OER polarization profiles of NC@Co-HPNC, Co-HPNC, Co-NC and RuO_2 in 1.0 M KOH solution at 1600 rpm.

As shown in **Fig. S17**, the NC@Co-HPNC catalyst exhibits an overpotential of 376.4 mV, which is smaller than these of the Co-HPNC (522.8 mV), Co-NC (426.2 mV) and RuO_2 (392.0 mV) catalysts, indicating the super-high activity of NC@Co-HPNC for OER. The superior OER activity of NC@Co-HPNC can also be demonstrated by its lowest Tafel slope (31.41 mV $decade^{-1}$) among all Co-based derivatives and commercial RuO_2.

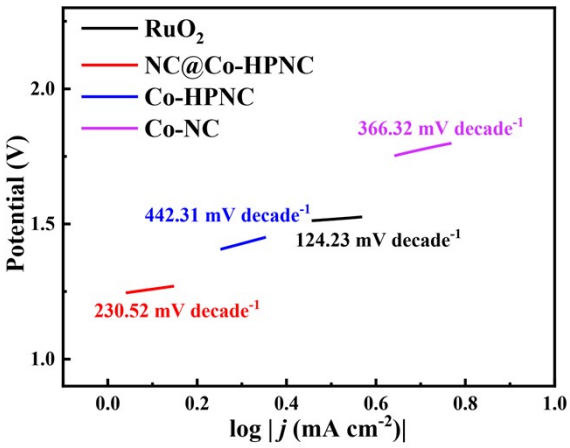

Fig. S18 OER polarization profiles corresponding Tafel plots of the RuO_2, NC@Co-HPNC, Co-HPNC and Co-NC catalysts in 0.5 M H_2SO_4 solution at 1600 rpm.

As shown in **Fig. S18**, NC@Co-HPNC shows the Tafel slope of 230.5 mV decade^{-1} in acid electrolyte, which is lower than that of Co-based materials but slightly higher than that of commercial RuO_2. These above results demonstrate that NC@Co-HPNC has relatively excellent catalytic property in 0.5 M H_2SO_4 electrolyte.

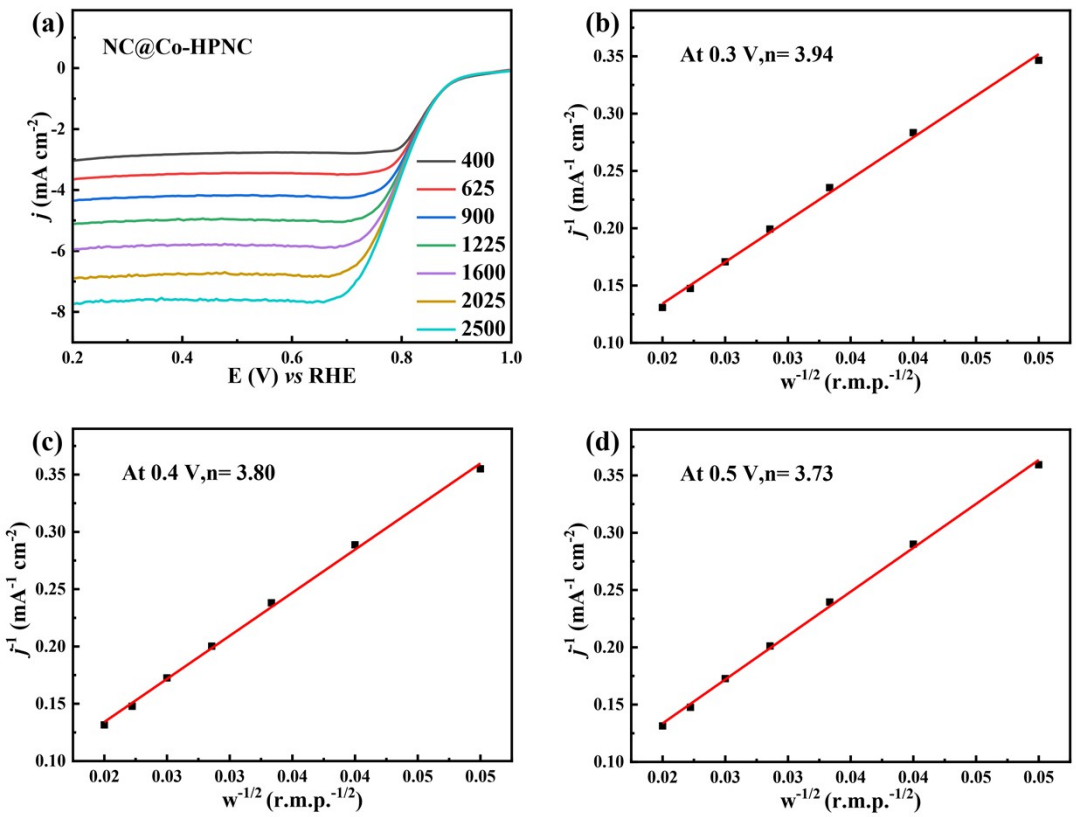

Fig. S19 (a) LSV curves of NC@Co-HPNC at different rotating speeds varying from 400 to 2500 rpm; The K–L plots obtained based on LSV of NC@Co-HPNC at different rotation speeds from 400 to 2500 rpm at various potentials: (b) 0.3 V, (c) 0.4 V and (d) 0.5 V.

As shown in **Fig. S19**, the ORR electron transfer kinetics of the NC@Co-HPNC catalyst was further investigated by recoding the LSV profiles at different rotating speeds from 400 to 2500 rpm. It can be observed from **Fig. S19** that the current density increases accordingly with the rotation speeds increasing and all the above LSVs exhibit good linearity and parallelism. Based on the Koutecky-Levich (K-L) equation and the above LSV curves, the average electron transfer number is ~3.82 under various voltages, which suggest that the ORR process of NC@Co-HPNC is 4-electron transfer pathway.

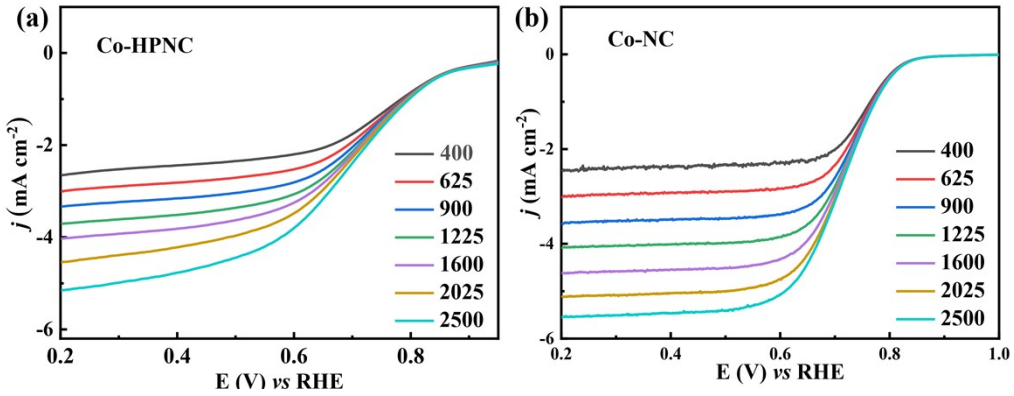

Fig. S20 LSV curves of (a) Co-HPNC and (b) Co-NC at different rotation speeds from 400 to 2500 rpm.

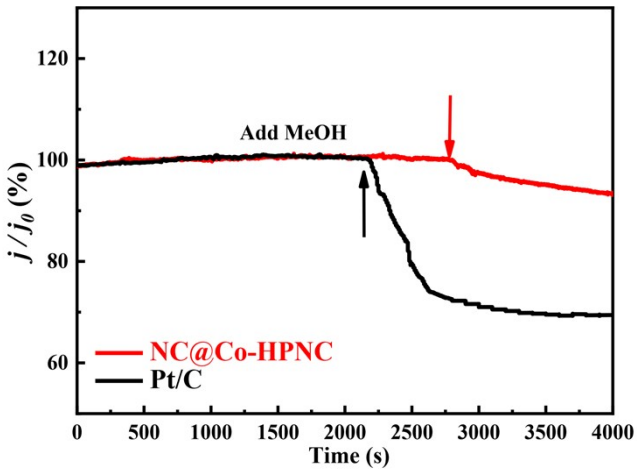

Fig. S21 ORR chronoamperometric responses of NC@Co-HPNC and Pt/C under the constant voltage (0.8 V *vs* RHE) after adding 5% (v/v) methanol addition in 0.1 M KOH solution at a speed of 1600 rpm.

It can be seen from **Fig. S21** that the ORR current of the NC@Co-HPNC catalyst only presents the slight attenuation, which reflects the excellent methanol tolerance of NC@Co-HPNC, comparing with the sharp drop in the current density of the Pt/C catalyst after injecting 5 % (volume of the electrolyte) methanol.

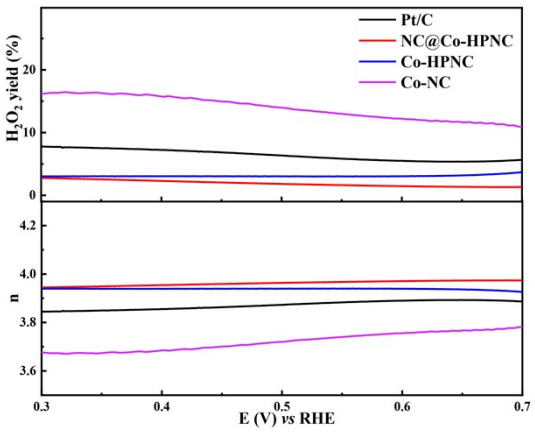

Fig. S22 Electron transfer numbers and H_2O_2 yield of Co-NC, Co-HPNC, NC@Co-HPNC and Pt/C.

Rotating ring disk electrode (RRDE) measurement was carried out to explore the activity of ORR on catalysts. It can be found from **Fig. S22** that the H_2O_2 yield of NC@Co-HPNC is only ~1.9 % and its corresponding electron-transfer number (n) is about 3.96 in 0.5 M H_2SO_4, while the Pt/C catalyst shows the H_2O_2 yield of ~2.0 % with n=3.95, further illustrating that the 4e pathway dominates the oxygen reduction process of NC@Co-HPNC.

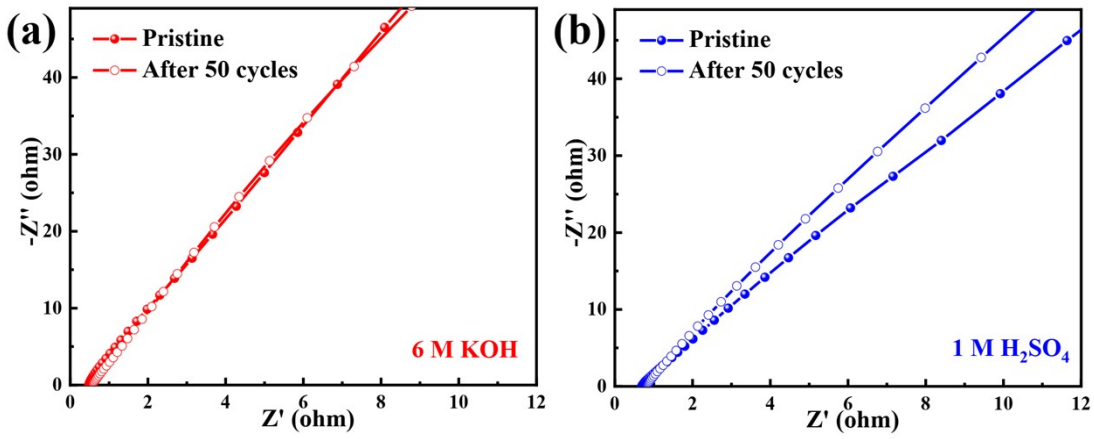

Figure S23 Nyquist plots of the (a) alkaline (6 M KOH) and (b) acid (1M H_2SO_4) electrolytes in the Zn–air cells using acid-base dual electrolyte before and after 50 cycles (Test conduction: at 1.0 mA cm^{-2} with a duration of 1h per cycle), two stainless steel sheets (SSS) are used and further coupled with the above electrolytes to form SSS/electrolyte/SSS symmetric cell and the measurement frequency ranges from 0.01 Hz to 100KHz.

It can be calculated from the Nyquist plots in **Figure S23a** and **b** that the Zn ionic conductivities of the pristine KOH and H_2SO_4 electrolytes are 37.43 and 26.00 mS cm^{-1}, while the Zn ionic conductivities of the cycled KOH and H_2SO_4 solutions are 31.46 and 21.69 mS cm^{-1}, respectively. These results indicate that the continuous discharge/charge processes only have a slightly effect on the ionic conductivity of alkaline (6 M KOH) and acid (1M H_2SO_4) electrolytes, which can be attributed to the typical structure of the Zn–air cells using acid-base dual electrolyte.

Tab. S1 The pore volume of NC@Co-HPNC, Co-HPNC and Co-NC.

Sample	**NC@Co-HPNC**	**Co-HPNC**	**Co-NC**
Pore volume (cm^3/g)	0.357	0.328	0.195

As shown in **Tab. S1**, the pore volume of NC@Co-HPNC is 0.357 cm^3 g^{-1}, which is higher compared with Co-NC (0.195 cm^3 g^{-1}) and Co-HPNC (0.328 cm^3 g^{-1}).

Tab. S2 The cycling performance comparison of the recently reported rechargeable Zn–air battery.

Catalysts	Cycle Number	Cycle Time (hour)	Average Overpotential (V)	Reference
$Co/ZnCo_2O_4$@NC -CNTs	258@5 mA cm^{-2}	103	~0.88 V	Ref. S1
CoMOF/LC-0.5	360@5 mA cm^{-2}	120	~0.7 V	Ref. S2
$Co(OH)_2$-$NiCo_2O_4$ /N-RGO	---@5 mA cm^{-2}	150	~0.9 V	Ref. S3
Fe-Co_4N@N-C	223@5 mA cm^{-2}	223	~0.8 V	Ref. S4
FeCo/Se-CNT	210@5 mA cm^{-2}	70	~0.8 V	Ref. S5
CoNC@N-CNF	380@5 mA cm^{-2}	63	~0.9 V	Ref. S6
CoO/Co_xP	400@5 mA cm^{-2}	200	~0.87 V	Ref. S7
NC@Co-HPNC	115@5 mA cm^{-2}	230	~0.75 V	This Work

As shown in **Tab. S2**, the NC@Co-HPNC cathodes displays the long cycling life of 230 h with the small average overpotentials (~0.75 V) at a current density of 5 mA cm^{-2}, which is better compared with the recently reported cathodes (**ref. S1-7**).

Tab. S3 The Co contents of the pristine and cycled NC@Co-HPNC catalysts measured by the inductively coupled plasma optical emission spectroscopy (ICP-OES) (Test conduction: operating 50 cycles at 1.0 mA cm^{-2} with duration of 1hour per cycle in the Zn–air cells using acid-base dual electrolyte).

Sample	Pristine	After cycling
NC@Co-HPNC	11.19 %	7.03 %

It can be found from **Table S3** that the Co mass contents of the pristine and cycled NC@Co-HPNC catalysts in the Zn–air cells using acid-base dual electrolyte are 11.19 and 7.03 %, respectively. Hence, the content of Co element in NC@Co-HPNC under acidic condition is also reduce, but the corresponding decrease is limited, which suggest that uniform carbon layer from PDA coating can inhibit the corrosion of Co-based nanoparticles to some extent in acid electrolyte.

Tab. S4 The operating voltages comparison for the recently reported different types of Zn–air battery.

Types of Zn–air batteries	Operating Voltage	Reference
Alkaline Zn−air batteries with FeNi/N-LCN	1.49 V	Ref. S8
Alkaline Zn−air batteries with FeS_2-CoS_2/NCFs	1.46 V	Ref. S9
Acidic Zn–air batteries with IrO_2@Ti	~2.0 V	Ref. S10
Alkaline Zn−air batteries with Fe-N-C	1.48 V	Ref. S11
Alkaline Zn−air batteries with NCNTM	1.50 V	Ref. S12
Acidic Zn–air battery with NC@Co-HPNC	>2.1 V	This Work

As shown in **Tab. S4**, the NC@Co-HPNC cathodes has an operating voltage of >2.1V, which is higher than most of the Zn–air batteries in recent works (**ref. S8-12**).

Reference

ref. S1: L. Yan, Z. Y. Xu, W. K. Hu, J. Q. Ning, Y. J. Zhong, Y. Hu, Formation of sandwiched leaf-like CNTs-Co/$ZnCo_2O_4$@NC-CNTs nanohybrids for high-power-density rechargeable Zn-air batteries, *Nano Energy*, **2021**, 82, 105710.

ref. S2: X. X. Wang, L. Ge, Q. Lu, J. Dai, D. Q. Guan, R. Ran, S. C. Weng, Z. W. Hu, W. Zhou, Z. P. Shao, High-performance metal-organic framework-perovskite hybrid as an important component of the air-electrode for rechargeable Zn-Air battery, *J. Power Sources*, **2020**, 468, 228377.

ref. S3: X. M. Peng, J. M. Zhang, T. L. Cen, Z. F. Ye, Y. Y. Liu, D. S. Yuan, $Co(OH)_2$-$NiCo_2O_4$ hybrid nanosheets coupled with N-doping reduced graphene oxide as efficient electrocatalysts for Zn-air batteries, *J. Alloys Compd.*, **2021**, 872, 159441.

ref. S4: Q. C. Xu, H. Jiang, Y. H. Li, D. Liang, Y. J. Hu, C. Z. Li, In-situ enriching active sites on co-doped Fe-Co_4N@N-C nanosheet array as air cathode for flexible rechargeable Zn-air batteries, *Appl. Catal. B: Environ.*, **2019**, 256, 117893.

ref. S5: H. W. Zhang, M. Q. Zhao, H. R. Liu, S. R. Shi, Z. H. Wang, B. Zhang, L. Song, J. Z. Shang, Y. Yang, C. Ma, L. R. Zheng, Y. H. Han, W. Huang, Ultrastable FeCo Bifunctional Electrocatalyst on Se-Doped CNTs for Liquid and Flexible All-Solid-State Rechargeable Zn−Air Batteries, *Nano Lett.*, **2021**, 21, 2255−2264.

ref. S6: W. M. Zhang, J. J. Chu, S. F. Li, Y. N. Li, L. Li, CoNxC active sites-rich three-dimensional porous carbon nanofibers network derived from bacterial cellulose and bimetal-ZIFs as efficient multifunctional electrocatalyst for rechargeable Zn–air

batteries, *J. Energ. Chem.*, **2020**, 51, 323–332.

ref. S7: Y. Niu, M. L. Xiao, J. B. Zhu, T. T. Zeng, J. D. Li, A "trimurti" heterostructured hybrid with an intimate CoO/CoxP interface as a robust bifunctional air electrode for rechargeable Zn–air batteries, *J. Mater. Chem. A*, **2020**, 8, 9177–9184.

ref. S8: X. F. Li, Y. J. Liu, H. B. Chen, M. Yang, D. G. Yang, H. M. Li, Z. Q. Lin, Rechargeable Zn−Air Batteries with Outstanding Cycling Stability Enabled by Ultrafine FeNi Nanoparticles-Encapsulated N-Doped Carbon Nanosheets as a Bifunctional Electrocatalyst, *Nano Lett.*, **2021**, 21, 3098−3105.

ref. S9: X. J. Shi, B. B. He, L. Zhao, Y. S. Gong, R. Wang, H. W. Wang, FeS2–CoS2 incorporated into nitrogen-doped carbon nanofibers to boost oxygen electrocatalysis for durable rechargeable Zn-air batteries, *J. Power Sources*, **2021**, 482, 228955.

ref. S10: L. J. Li, A. Manthiram, Long-Life, High-Voltage Acidic Zn–Air Batteries, *Adv. Energy Mater.*, **2016**, 6, 1502054.

ref. S11: D. Wang, H. Xu, P. X. Yang, L. H. Xiao, L. Du, X. Y. Lu, R. P. Li, J. Q. Zhang, M. Z. An, A dual-template strategy to engineer hierarchically porous Fe–N–C electrocatalysts for the highperformance cathodes of Zn–air batteries, *J. Mater. Chem. A*, **2021**, 9, 9761.

ref. S12: G. D. Chen, Y. Y. Xu, L. Huang, A. I. Douka, B. Y. Xia, Continuous nitrogen-doped carbon nanotube matrix for boosting oxygen electrocatalysis in rechargeable Zn-air batteries, *J. Energy Chem.*, **2021**, 55, 183–189.